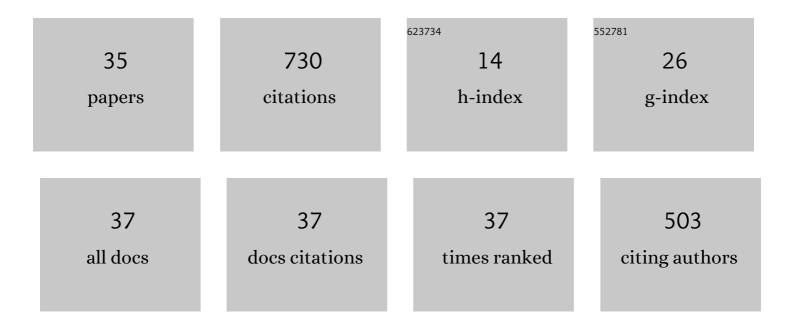
## Jonathan Mamou

List of Publications by Year in descending order

Source: https://exaly.com/author-pdf/6898947/publications.pdf Version: 2024-02-01



#	Article	IF	CITATIONS
1	Vitrectomy Improves Contrast Sensitivity in Multifocal Pseudophakia With Vision Degrading Myodesopsia. American Journal of Ophthalmology, 2022, 244, 196-204.	3.3	3
2	Quantitative Ultrasound Assessment of Early Osteoarthritis in Human Articular Cartilage Using a High-Frequency Linear Array Transducer. Ultrasound in Medicine and Biology, 2022, 48, 1429-1440.	1.5	1
3	Biomechanical changes in myopic sclera correlate with underlying changes in microstructure. Experimental Eye Research, 2022, 224, 109165.	2.6	1
4	A Deep Learning Approach for Segmentation, Classification and Visualization of 3D High Frequency Ultrasound Images of Mouse Embryos. IEEE Transactions on Ultrasonics, Ferroelectrics, and Frequency Control, 2021, 68, 1-1.	3.0	8
5	Autoregressive Model-Based Reconstruction of Quantitative Acoustic Maps From RF Signals Sampled at Innovation Rate. IEEE Transactions on Computational Imaging, 2020, 6, 993-1006.	4.4	1
6	Deep Mouse: An End-to-End Auto-Context Refinement Framework for Brain Ventricle & Body Segmentation in Embryonic Mice Ultrasound Volumes. , 2020, 2020, 122-126.		7
7	Scanner Independent Deep Learning-Based Segmentation Framework Applied to Mouse Embryos. , 2020, ,		1
8	Regional changes in the elastic properties of myopic Guinea pig sclera. Experimental Eye Research, 2019, 186, 107739.	2.6	7
9	Automatic Mouse Embryo Brain Ventricle & Body Segmentation and Mutant Classification From Ultrasound Data Using Deep Learning. , 2019, , .		5
10	Cerebellar folding is initiated by mechanical constraints on a fluid-like layer without a cellular pre-pattern. ELife, 2019, 8, .	6.0	26
11	Deep Bv: A Fully Automated System for Brain Ventricle Localization and Segmentation In 3D Ultrasound Images of Embryonic Mice. , 2018, 2018, .		9
12	Improved High-Frequency Ultrasound Corneal Biometric Accuracy by Micrometer-Resolution Acoustic-Property Maps of the Cornea. Translational Vision Science and Technology, 2018, 7, 21.	2.2	6
13	Autoregressive Signal Processing Applied to High-Frequency Acoustic Microscopy of Soft Tissues. IEEE Transactions on Ultrasonics, Ferroelectrics, and Frequency Control, 2018, 65, 2054-2072.	3.0	15
14	Automatic body localization and brain ventricle segmentation in 3D high frequency ultrasound images of mouse embryos. , 2018, 2018, 635-639.		7
15	A Novel Quantitative 500-MHz Acoustic Microscopy System for Ophthalmologic Tissues. IEEE Transactions on Biomedical Engineering, 2017, 64, 715-724.	4.2	36
16	Regular chondrocyte spacing is a potential cause for coherent ultrasound backscatter in human articular cartilage. Journal of the Acoustical Society of America, 2017, 141, 3105-3116.	1.1	7
17	Acoustic Impedance Analysis with High-Frequency Ultrasound for Identification of Fatty Acid Species in the Liver. Ultrasound in Medicine and Biology, 2017, 43, 700-711.	1.5	21
18	Segmentation of 3-D High-Frequency Ultrasound Images of Human Lymph Nodes Using Graph Cut With Energy Functional Adapted to Local Intensity Distribution. IEEE Transactions on Ultrasonics, Ferroelectrics, and Frequency Control, 2017, 64, 1514-1525.	3.0	7

**JONATHAN ΜΑΜΟ** 

#	Article	IF	CITATIONS
19	Material Properties of Human Ocular Tissue at 7-µm Resolution. Ultrasonic Imaging, 2017, 39, 313-325.	2.6	11
20	Local Transverse-Slice-Based Level-Set Method for Segmentation of 3-D High-Frequency Ultrasonic Backscatter From Dissected Human Lymph Nodes. IEEE Transactions on Biomedical Engineering, 2017, 64, 1579-1591.	4.2	11
21	Effects of Signal Saturation on QUS Parameter Estimates Based on High-Frequency-Ultrasound Signals Acquired From Isolated Cancerous Lymph Nodes. IEEE Transactions on Ultrasonics, Ferroelectrics, and Frequency Control, 2017, 64, 1501-1513.	3.0	2
22	Quantitative Characterization of Tissue Microstructure in Concentrated Cell Pellet Biophantoms Based on the Structure Factor Model. IEEE Transactions on Ultrasonics, Ferroelectrics, and Frequency Control, 2016, 63, 1321-1334.	3.0	25
23	Microstructural assessment of the guinea pig sclera using quantitative acoustic microscopy. , 2016, , .		3
24	Speed of sound in diseased liver observed by scanning acoustic microscopy with 80 MHz and 250 MHz. Journal of the Acoustical Society of America, 2016, 139, 512-519.	1.1	32
25	Nested Graph Cut for Automatic Segmentation of High-Frequency Ultrasound Images of the Mouse Embryo. IEEE Transactions on Medical Imaging, 2016, 35, 427-441.	8.9	22
26	Acoustic-property maps of the cornea for improved high-frequency ultrasound corneal biometric accuracy. , 2015, , .		6
27	Automatic mouse embryo brain ventricle segmentation, gestation stage estimation, and mutant detection from 3D 40-MHz ultrasound data. , 2015, , .		5
28	Fine-resolution elastic-property maps of myopic sclera by means of acoustic microscopy. , 2015, , .		5
29	Fine-resolution maps of acoustic properties at 250 MHz of unstained fixed murine retinal layers. Journal of the Acoustical Society of America, 2015, 137, EL381-EL387.	1.1	25
30	High-Throughput, High-Frequency 3-D Ultrasound for in Utero Analysis of Embryonic Mouse Brain Development. Ultrasound in Medicine and Biology, 2013, 39, 2321-2332.	1.5	33
31	Three-dimensional quantitative ultrasound for detecting lymph node metastases. Journal of Surgical Research, 2013, 183, 258-269.	1.6	34
32	Three-Dimensional High-Frequency Backscatter and Envelope Quantification of Cancerous Human Lymph Nodes. Ultrasound in Medicine and Biology, 2011, 37, 345-357.	1.5	139
33	Three-Dimensional High-Frequency Characterization of Cancerous Lymph Nodes. Ultrasound in Medicine and Biology, 2010, 36, 361-375.	1.5	84
34	Extended three-dimensional impedance map methods for identifying ultrasonic scattering sites. Journal of the Acoustical Society of America, 2008, 123, 1195-1208.	1.1	47
35	Identifying ultrasonic scattering sites from three-dimensional impedance maps. Journal of the Acoustical Society of America, 2005, 117, 413-423.	1.1	75